Published in final edited form as:
Structure. 2012 August 8; 20(8): . doi:10.1016/j.str.2012.03.027.

Mechanism of Cd^{2+}-coordination during Slow Inactivation in Potassium Channels

H. Raghuraman[1], **Julio F. Cordero-Morales**[1,2], **Vishwanath Jogini**[1,3], **Albert C. Pan**[1,4], **Astrid Kollewe**[5], **Benoît Roux**[1], and **Eduardo Perozo**[1]

[1]Department of Biochemistry and Molecular Biology, The University of Chicago, Chicago, Ilinois, USA

[2]Department of Physiology, University of California San Francisco, San Francisco, California, USA

[3]D. E. Shaw Research, Hyderabad, India

[4]D. E. Shaw Research, New York, New York USA

[5]University of Freiburg, Dept. of Physiology II, Freiburg, Germany

Summary

In K^+ channels, rearrangements of the pore outer-vestibule have been associated with C-type inactivation gating. Paradoxically, the crystal structure of Open/C-type inactivated KcsA suggest these movements to be modest in magnitude. Here, we show that under physiological conditions, the KcsA outer-vestibule undergoes relatively large dynamic rearrangements upon inactivation. External Cd^{2+} enhances the rate of C-type inactivation in an outer-vestibule cysteine mutant (Y82C) via metal-bridge formation. This effect is not present in a non-inactivating mutant (E71A/Y82C). Tandem dimer and tandem tetramer constructs of equivalent cysteine mutants in KcsA and *Shaker* K^+ channels demonstrate that these Cd^{2+} metal bridges are formed only between adjacent subunits. This is well supported by molecular dynamics simulations. Based on the crystal structure of Cd^{2+}-bound Y82C-KcsA in the closed state, together with EPR distance measurements in the KcsA outer-vestibule, we suggest that subunits must dynamically come in close proximity as the channels undergo inactivation.

Introduction

In K^+ channels, stimulus-dependent activation is associated with conformational changes around a gating hinge at the inner helix bundle (Perozo et al., 1998; 1999; Yellen, 1998; Blunk et al., 2006; Cordero-Morales et al., 2006b; Jiang et al., 2002; Long et al., 2005; Alam and Jiang, 2009; Cuello et al., 2010a). However, in response to prolonged stimulus and in the absence of an N-terminal inactivating particle, most K^+ channels become nonconductive through a process known as C-type inactivation, first identified in *Shaker* K^+ channels (Hoshi et al., 1990; 1991; Kurata and Fedida, 2006). This C-type inactivation is crucial in controlling the firing patterns in excitable cells (Bean, 2007) and is fundamental in determining the length and frequency of the cardiac action potential (Smith et al., 1996; Spector et al., 1996). It is therefore an effective mechanism for controlling the duration of

Correspondence should be addressed to: E.P (eperozo@uchicago.edu).

Supplemental Information: Supplemental information includes one figure, and 2 movies and can be found with this article online.

Accession Numbers: The atomic coordinates of the Cd^{2+}-bound and spin label-bound Y82C-KcsA have been deposited in the Protein Data Bank under accession codes 3STL and 3STZ, respectively.

the conductive state through structural rearrangements along the permeation pathway (Yellen, 1998; Hoshi et al., 1991). C-type inactivation is affected by high extracellular K^+ and the blocker tetraethylammonium (TEA) (Baukrowitz and Yellen, 1995; Lopez-Barneo et al., 1993; Choi et al., 1991) and can also be modulated by permeant ions with a long residence time in the selectivity filter (Rb^+, Cs^+ and $NH4^+$) (Swenson and Armstrong, 1981; Demo and Yellen, 1992). It is now firmly established that C-type inactivation is associated with the conformational changes at the selectivity filter and the outer-vestibule of K^+ channel (Cordero-Morales et al., 2006a; 2006b; 2007; Cuello et al., 2010a; Chakrapani et al., 2011; Claydon et al., 2003; Berneche and Roux, 2005; Yellen et al., 1994; Liu et al., 1996; Cha and Bezanilla, 1997; Schlief et al., 1996; Ader et al., 2008). In the pH-gated K^+ channel KcsA, it has been shown that there is a remarkable correlation between the degree of activation gate opening and the conformation and occupancy of the selectivity filter (Cuello et al., 2010). In addition, disrupting the hydrogen-bond network (Glu71-Asp80 interaction in particular) behind the selectivity filter in KcsA relieves C-type inactivation, and this has resulted in identification of the non-inactivating E71A mutant (Cordero-Morales et al., 2006b).

Mutations at the outer-vestibule of *Shaker*, a voltage-gated K^+ channel from *Drosophila*, identified an important role for Thr449 in the regulation of C-type inactivation (Lopez-Barneo et al., 1993; Yellen et al., 1994). Metal-binding experiments showed that cysteine substitution of T449 in the outer-vestibule of *Shaker* (just above the selectivity filter) allowed the modulation of C-type inactivation by the extracellular divalent cations such as Cd^{2+} and Zn^{2+}. In addition, the rate of modification of several substituted cysteine residues in the outer-vestibule by thiol-reactive agents is significantly increased when the channels undergo C-type inactivation (Liu et al., 1996). Interestingly, the time-dependence of conformational changes near the T449C residue and other residues in the outer-vestibule of the channel approximates the time course of C-type inactivation (Cha and Bezanilla, 1997; Loots and Isacoff, 1998; 2000; Gandhi et al., 2000). These results clearly suggest a conformational rearrangement in the outer-vestibule (around the T449 residue) during C-type inactivation in *Shaker* channels. However, recent crystal structures of open-inactivated KcsA display only modest conformational changes in the outer-vestibule (Cuello et al., 2010a), an intriguing fact that requires alternative explanations to the metal bridge results.

To understand the molecular basis of events associated with C-type inactivation and high affinity Cd^{2+} binding, we set off to determine the topology of Cd^{2+} coordination state in the transition between the closed, open and inactivated states of K^+ channels. We made a cysteine substitution in the Tyr82 residue of the outer-vestibule of KcsA, equivalent to Thr449 in *Shaker* channels. We then compared the effect of Cd^{2+} in two different functional states of KcsA, using inactivating (wild-type) and non-inactivating (E71A) backgrounds to monitor the gating-related rearrangements in the outer-vestibule, and extend our findings to *Shaker* K^+ channels. Based on our findings, we propose that the formation of metal bridge is crucial to affect the rate of inactivation and abrogates ion conduction in K^+ channels. The metal bridge formation occurs between adjacent subunits, which requires the subunits come closer dynamically during inactivation gating of KcsA. This mechanism appears to be consistent with structural changes associated with C-type inactivation in eukaryotic voltage-dependent K^+ channels and should further increase our understanding of the importance of structural dynamics at the K^+ channel outer-vestibule during inactivation gating.

Results

Cd^{2+} Facilitates the Rate of Inactivation of KcsA

We have engineered a cysteine mutant in the outer-vestibule residue of KcsA (Y82), just above the selectivity filter to monitor the gating-related structural rearrangements and pore

geometry. Y82C is equivalent to T449C in *Shaker* potassium channels, which has been shown to significantly alter the C-type inactivation (Yellen et al., 1994). Further, a tyrosine residue at this position in the outer-vestibule is conserved among other voltage-gated K^+ channels such as $K_v2.1$ and $K_v3.1$ (Shealy et al., 2003). Macroscopic electrophysiological recordings using pH jump measurements show that the rate of inactivation of Y82C is similar to wild type KcsA (Cordero-Morales et al., 2006b) with an inactivation time constant of ∼1200 ms (Figure 1A). At low concentrations of Cd^{2+} (10 μM), the inactivation time constant remains invariant (Figure 1B). Interestingly, as the concentration of Cd^{2+} is increased in the pipette, it facilitates the inactivation of channels with a mid-point around 40 μM (τ_i = ∼120 ms; Figure 1A-E). Cd^{2+} does not have any effect on the inactivation rate of WT KcsA (not shown), suggesting that Cd^{2+} interacts specifically with the cysteine introduced at the outer-vestibule of KcsA (Y82C). The inactivation time constant of Y82C-KcsA as a function of increasing Cd^{2+} concentrations is shown in Figure 1E. There is a 10-fold increase in the rate of inactivation in the presence of Cd^{2+}, which is in excellent agreement with *Shaker* T449C results in which it was shown that the presence of Cd^{2+} increases the forward rate of inactivation by 10-fold, *i.e*., from 1600 ms to 160 ms in the presence of 300 μM of Cd^{2+} (Yellen et al., 1994). It should be noted that the liposome patches we used for monitoring the effect of Cd^{2+} on C-type inactivation of KcsA channels are ‘inside-out’ patches. Once these ‘inside-out’ patches have been made, we do not have direct access to exchanging buffers in the pipette and the channels are trapped in the inactivated conformation (especially in the presence of Cd^{2+}). Therefore, individual patches have been used to study the effect of Cd^{2+} concentration on the rate of inactivation of KcsA. Since we observed a 10-fold difference in the time constant of inactivation in KcsA similar to *Shaker* using less Cd^{2+} (100 μ M), we expect the recovery from inactivation might be comparable to *Shaker*. Because Cd^{2+} binds with high affinity to inactivated channels, we tested the effect of Cd^{2+} on the non-inactivating (E71A) mutant background of KcsA. Importantly, there is no effect of Cd^{2+} in the non-inactivating mutant (E71A) background even at the highest concentration studied, *i.e*., 1 mM (Figure 1F). This indicates that the conformation of the outer-vestibule in non-inactivating channels could be different and also suggests that the Cd^{2+} metal bridge could form only in channels that undergo inactivation.

To understand the conformational differences in the outer-vestibule of inactivating and non-inactivating channels, we performed CW-EPR spectroscopy. The spin-labeled Y82C channel in both wild-type and E71A backgrounds has a broad spectrum with a significant spin-spin coupling in the closed state (Figure 2). This is expected if the Y82C residues are in close proximity with each other irrespective of whether the Y82C channel is in WT or in E71A (non-inactivated) backgrounds. Although there is no significant spectral change for Y82C-SL upon opening the activation gate (Figure 2A), the non-inactivating Y82C-SL/E71A construct shows a spectrum with much reduced spin-spin coupling and a profound increase in the mobility of Y82C residues (Figure 2B). We have taken this result as evidence for a highly flexible outer-vestibule in the conductive state. This enhanced flexibility would lead to an increased average distance among Y82C residues in non-inactivated channels, a likely explanation for the inability of E71A channels to form Cd^{2+} metal bridges (Figure 1F). This result might be directly related to the structure of ‘flipped’ E71A (Cordero-Morales et al., 2006b), which exemplifies the conformational differences of the Y82 side chain in the outer-vestibule in non-inactivating channels (see Figure S1).

Topology of Cd^{2+} Coordination States

Although Cd^{2+} stabilizes the inactivated state of a channel, the exact mechanism by which the Cd^{2+} metal bridge is formed is not well understood. It was postulated that either a Cd^{2+} ion can occupy the centre of the channel just above the pore (coordinated by four cysteines of different subunits) or that the accessibility of the cysteine residues could be different in

inactivated channels (Yellen et al., 1994). Genetically linked tandem constructs have been successfully used to study the cooperativity of gating and block in K^+ channels (Heginbotham and MacKinnon, 1992; Hurst et al., 1992; Ogielska et al., 1995; Yang et al., 1997). Previous work from our lab has shown wild type-like stability and function for tandem dimer (TD) (Liu et al., 2001) and tandem tetramer (TT) (Liu, 2004) KcsA channels. These constructs provide us with opportunity to place cysteines exclusively in the subunit(s) of interest to dissect the mechanism of Cd^{2+} coordination during inactivation gating.

Two types of constructs were made: TD-Y82C where the KcsA tetramer has only two cysteines placed in two diagonally symmetric subunits, and TT-Y82C constructs in which the cysteines can be placed in adjacent subunits. A schematic representation of the TD and TT constructs is shown in Figure 3. Cd^{2+} experiments show that in TD-Y82C constructs (Figure 3A) the inactivation time constant is similar in the presence and absence of saturating concentrations of Cd^{2+} (τ_i = ~1100 ms). However, when the cysteines are placed in adjacent subunits (TT-Y82C), the presence of Cd^{2+} leads to faster inactivation (τ_i ~250 ms) (Figure 3B). These results demonstrate that only cysteines placed in adjacent subunits are geometrically adept at forming a Cd^{2+} metal bridge, thus ruling out the possibility of central coordination of Cd^{2+} as previously proposed (Yellen et al., 1994). Further, it should be noted that while only 2 cysteines are available to participate in metal bridge formation in these TT channels, the inactivation rate is comparable to four-cysteine channels (τ_i ~120 ms, see Figure 1).

To evaluate the energetic stability of Cd^{2+} coordinated states, we performed molecular dynamics simulations using the low K^+ high-resolution structure (PDB: 1K4D) (Zhou et al., 2001) as a template to the inactivated Y82C channel *in silico*. The selectivity filter in low K^+ KcsA structure is collapsed with only 2 ions in the binding site and is structurally close to the inactivated state (Cuello et al., 2010a). When Cd^{2+} is placed between adjacent subunit cysteines, the Cd^{2+} - cysteines (γ -Sulfur) distances remain constant at ~2.5 Å during the simulation (Figure 4A, top panel). In contrast, an attempt to coordinate a Cd^{2+} between diagonally opposing subunits led to a dramatic change in the Cd^{2+} - cysteines distance. In this simulation, Cd^{2+} binds to a cysteine of one subunit and the other subunit moves apart in <20 ps of simulation (Figure 4A, bottom panel). A snapshot of each coordination state is also shown for comparison in Figure 4A. These results clearly demonstrate that the metal bridge formation between adjacent subunits is the most stable topology for Cd^{2+} coordination states, and the formation of Cd^{2+} metal bridge is not stable between two diagonally symmetric subunits. Further, we calculated the free energy associated with the movement of Cd^{2+} from the initially placed stable coordination between adjacent subunits until the coordination between opposing subunits is achieved. Snapshots of Cd^{2+} bound states along the trajectory of movement of Cd^{2+} from adjacent cysteines to opposing subunits are shown in Figure 4B, which illustrates the high energetic penalty (~50 Kcal/mol) involved in the movement of Cd^{2+} to form a metal bridge between opposing subunits (Movies S1 and S2).

Crystal Structure of Cd^{2+}-bound Y82C-KcsA

In an attempt to visualize the Cd^{2+} coordinated state in Y82C-KcsA, the Cd^{2+} bound form of Y82C channel was crystallized by co-crystallization or Cd^{2+} (100 μM) soaking experiments after formation of crystals. The structure of Cd^{2+} bound Y82C channel in the closed state was determined at 2.4 Å resolution using Fab fragments (Figure 5). Surprisingly, the structure shows no explicit metal bridges, as four Cd^{2+} appear bound to individual cysteine residues. Interestingly, the S_γ-S_γ distance between cysteine residues among diagonal and adjacent subunits in the Cd^{2+} bound Y82C structure is 16.5 Å and 11.7 Å, respectively (Figure 5). Clearly the cysteine residues are very far when compared to the distance needed

to form a Cd^{2+} metal bridge (~5 Å) (Narula et al., 1995; Naylor et al., 1998). This structure might therefore represent the low affinity Cd^{2+} bound conformation in the closed state and also might suggest that the inactivation is followed by Cd^{2+} binding. Since prior opening of the channel is necessary for the subsequent transition to the inactivated state (Yellen et al., 1994), it is possible that the conformation of outer-vestibule may not allow Cd^{2+} metal bridge formation especially in the presence of Fab fragments as the antibody substantially reduces inactivation and stabilizes the channel in its conductive conformation (Cordero-Morales et al., 2006b). The presence of antibody is therefore likely to limit the outer-vestibule conformational flexibility, and this might not allow the Cd^{2+} metal bridge to form. Attempts to crystallize Cd^{2+} bound form in the non-conductive conformation of the filter using low K^+ conditions or the M96V background (Lockless et al., 2007) were unsuccessful.

Subunits Come Closer Dynamically during Inactivation Gating

Considering the Cd^{2+}-induced change in the inactivation rate and the structure of Cd^{2+}-bound Y82C in the closed state, it is conceivable that the outer-vestibule must undergo a significant conformational change during inactivation gating. Conformational changes might include the change in dynamic accessibility of cysteine residues (Yellen et al., 1994; Liu et al., 1996) or the change in the geometry of outer-vestibule due to change in proximity of subunits. We have utilized the sensitivity of CW-EPR to dipolar interactions to monitor the distance between spin labeled Y82C residues in the symmetric diagonal subunits (Liu et al., 2001) under conditions that promote entry to the conductive and non-conductive forms of the filter.

Since KcsA is a homotetramer, distance measurements based on spin-spin interactions are complicated by the geometric relationship among subunits. A fully spin-labeled channel will show dipolar interactions between adjacent and diagonally related subunits. Although the coupling among the adjacent subunits will be the predominant contributor to spectral broadening, diagonally related residues close to the four-fold axis of symmetry will also show substantial broadening effects. We therefore used TD-Y82C constructs, which will generate a channel with only two spin labels in diagonally opposing subunits, eliminating the dipolar interactions from adjacent subunits (Liu et al., 2001).

The fully labeled and under labeled EPR spectra of membrane reconstituted TD-Y82C along with the distance distributions in the closed and open activation gates are shown in Figure 6. Assuming a single Gaussian distribution, the mean distance obtained between spin labels in TD-Y82C when the lower gate is closed is 12 Å (Figure 6A, top). To validate the experimentally determined mean distance, we crystallized the spin label-bound Y82C-KcsA using Fab at 2.5 Å (Figure 6B). The electron density of the selectivity filter with spin label-bound Y82C is shown for two diagonally symmetric subunits (Figure 6B, right) along with the top view of the spin labeled structure (Figure 6B, left). The distance extracted from the crystal structure between the two nitroxide spin labels in diagonal subunits is 12.7 Å, which is in excellent agreement with the EPR determined mean distance between the spin labels in the TD Y82C channels in the closed state (12 Å). Upon opening the activation gate, the distance between the two spin labels in TD-Y82C channels is found to be 8 Å (Figure 6A, bottom), clearly 2 Å inward movement for each subunit. This is consistent with our Cd^{2+} binding experiments and also with previous reports showing that dynamic structural rearrangements occur in the outer-vestibule of voltage-gated potassium channels during inactivation gating (Yellen et al., 1994; Liu et al., 1996).

To what extent does the Cd^{2+} coordination during inactivation gating in KcsA relate to equivalent events in eukaryotic K^+ channels? To answer this question, various tandem tetramer *Shaker*-IR T449C constructs were expressed in *Xenopus laevis* oocytes and examined using two-electrode voltage clamp under the same conditions as those for KcsA.

Figure 7 shows the whole-cell currents from T449C mutant of ShΔ in the absence and presence of Cd^{2+} and its dependence on the position of cysteines. When only one subunit has the T449C mutation (Figure 7A, E), Cd^{2+} does not show any effect on inactivation suggesting that although Cd^{2+} can bind individual cysteine (see Figure 5), the formation of Cd^{2+} metal bridge is an absolute necessity to exert Cd^{2+}-induced inactivation. Cd^{2+} exerts a significant increase in the rate and extent of inactivation when two cysteines are placed in adjacent subunits with ∼55% inhibition of K^+ current. This is in good agreement with the results of TT-Y82C-KcsA where the cysteines are placed only in adjacent subunits (Figure 3B). Interestingly, Cd^{2+} causes a small effect on rate of inactivation (∼20% reduction in current) in *Shaker*-IR T449C constructs where the cysteines are placed only on diagonal subunits (Figure 7B), which is suggestive of some formation of Cd^{2+} metal bridge between diagonal subunits. However, this was not observed in KcsA (Figure 3A). This small discrepancy between KcsA and ShΔ with respect to the Cd^{2+} coordination between opposing subunits could be due to different organization or the intrinsic dynamics of the outer-vestibule in ShΔ channels. Nevertheless, we propose that the probability of forming the metal bridge between adjacent subunits is highly favorable in K^+ channels and likely drives most of current reduction and stabilization of C-type inactivated state seen previously (Yellen et al., 1994).

Discussion

Many compounds alter the function of ion channels by modulating their gating behavior, and metal ions such as Cd^{2+} and Zn^{2+} in particular have been widely used to determine the structural organization of the outer mouth and pore geometry in a variety of channels during gating (Yellen et al., 1994; Elinder and Arhem, 2004; Sobolevsky et al., 2004; Szendroedi et al., 2007). It has been shown that in *Shaker* T449C, Cd^{2+} increases the inactivation rate by ∼10 fold, and the metal ion has ∼45,000 fold higher affinity for the inactivated channels upon transition from the open state (Yellen et al., 1994). Here, we show that in Y82C-KcsA, Cd^{2+} facilitates the inactivation in a concentration dependent manner (see Figure 1E) which points out to a mechanistic equivalence between KcsA inactivation and C-type inactivation in voltage-gated K^+ channels (Lopez-Barneo et al., 1993; Yellen et al., 1994; Cordero-Morales et al., 2006a; 2006b; 2007; Cuello et al., 2010b). Interestingly, in the non-inactivating form of KcsA (Y82C in the E71A background), Cd^{2+} exerts no effect on the ionic currents (Figure 1E), suggesting that the constriction of the outer-vestibule is less explicit in the open, non-inactivating state of KcsA. This also highlights the conformational differences in the outer-vestibule between the conductive and C-type inactivated forms of KcsA, as supported by EPR measurements (Figure 2).

We have used tandem constructs, EPR spectroscopy, X-ray crystallography and computational analysis to investigate the molecular mechanisms underlying the role of the K^+ channel external vestibule in C-type inactivation while addressing the Cd^{2+} inhibition paradox. To elucidate the mechanism of Cd^{2+} coordination during inactivation gating, we measured K^+ currents in an inside-out patch in proteoliposomes made of tandem dimer and tandem tetramer constructs in which the Y82C mutation is placed diagonally and adjacently placed cysteines, respectively. The results showed that outer-vestibule conformational changes associated with C-type inactivation favors the formation of Cd^{2+} metal bridges between adjacent subunits with minimal contribution of diagonally located subunits (Figure 3). This is consistent with our results obtained in ShΔ constructs expressed in oocytes (Figure 7) and with a previous report, which suggests that residue Thr449 does not move toward the center of the conduction pathway during inactivation (Andalib et al., 2004). A similar Cd^{2+} coordination configuration between adjacent subunits has been proposed for the outer pore of the glutamate receptor channel (Sobolevsky et al., 2004). Molecular dynamic simulation results, using the low K^+ structure as a model for the inactivated

selectivity filter, support our observations and suggest that while Cd^{2+} coordination between the adjacent subunits is very stable, the formation of a Cd^{2+} metal bridge between diagonal subunits is energetically unfavorable (by as much as ∼50 Kcal/mol, see Figure 4). Overall, these results favor a model in which two Cd^{2+} ions coordinated by the cysteines of adjacent subunits, and argue against a single Cd^{2+} being coordinated by four cysteines (Yellen et al., 1994) on the basis of simple geometric constraints.

High-resolution structures of the Cd^{2+} coordination complexes in proteins suggest that the expected distance between Cd^{2+} and the Sγ of cysteines is ∼2.5 Å (Narula et al., 1995; Naylor et al., 1998), placing an optimum distance for coordinating cysteines in a Cd^{2+} metal bridge near ∼5 Å. Interestingly, the crystal structure of Cd^{2+}-bound to Y82C-KcsA in the closed state shows that under the present crystallization conditions Cd^{2+} binds to individual cysteines in the closed state, with no evidence for inter-subunit metal bridges (Figure 5). This shows that the cysteine side chains in Y82C position are easily accessible to reactive agents (see also Figure 2 for accessible to relatively bulky nitroxide spin label), and rules out an earlier report (Liu et al., 1996) suggesting that the side chains of T449C mutant in *Shaker* K^+ channel might be hidden from the aqueous pore in the closed state. We could never observe a Cd^{2+} metal bridge in the closed state under a variety of conditions (low K^+, M96V background) a fact that strongly suggests that the pore geometry in the closed state could be different compared to the open, inactivated conformation. In this structure, the distance between the cysteines S_γ in diagonal and adjacent subunits is 16.5 Å and 11.7 Å, respectively, clearly far from the distance needed to form a Cd^{2+} bridge and implies that there has to be a significant change in the outer-vestibule of KcsA during inactivation gating to bring the cysteines of adjacent subunits to ∼5 Å. In other words, the subunits must come close together during the transition from closed conductive to open inactivated conformation through the open conductive state. Indeed, distance measurements using spin labeled tandem dimer Y82C-KcsA constructs clearly demonstrate that the subunits come close together during inactivation gating (see Figure 6A), which would favor the formation of a metal bridge between adjacent subunits. Though the subunits come close together during inactivation gating, the distance of ∼8 Å between diagonal subunits in the open, inactivated state (Figure 6A, bottom) is still too long to favor Cd^{2+} coordination. Taken together, these results suggest the higher affinity of Cd^{2+} binding in the outer mouth of K^+ channels in the inactivated state between adjacent subunits is predominantly due to the change in pore geometry caused by the change in dynamics and proximity of subunits rather than change in accessibility of side chains (Liu et al., 1996).

It is surprising to note that though our results clearly show that the subunits come closer during inactivation gating, the crystal structures of open/C-type inactivated KcsA do not show any significant conformational changes in the outer-vestibule (Cuello et al., 2010a). One possible explanation could be that there are two independent conformational ‘triggers’ of the filter inactivation gate – one at the outer-vestibule and the other at the cytoplasmic activation gate. However, we believe that the conformational changes with the outer-vestibule is associated with the activation gate opening because we have previously shown that the presence of antibody substantially reduces inactivation and stabilizes the channel in its conductive conformation in reconstituted WT-Fab complex (Cordero-Morales et al., 2006a). In the presence of antibody, the outer vestibule might adopt the Fab-stabilized conformation. This might explain the absence of significant changes in the outer-vestibule of X-ray structures of open/C-type inactivated KcsA. The same is the case with the crystal structure of KcsA-Fab complex at low K^+ concentration (Zhou et al., 2001). Further, in case of spin labeled Y82C channel in wild type, the observation that there is no significant spectral change upon opening the lower gate cannot be taken as an evidence for two independent conformational ‘triggers’ for the filter inactivation. The spin-labeled Y82C channel in wild-type has a broad spectrum with a significant spin-spin coupling in both

closed and open states (Fig. 2A). We know, from distance measurements, that the average distance between spin labels is ∼10 Å (diagonal = ∼12 Å as determined by distance measurements and observed in Y82C-SL crystal structure; adjacent = ∼ 8.5 Å estimated from symmetry constraints). Since the EPR spectrum is already severely broadened in the closed state due to the close proximity of spin labels as well as restricted mobility, the spectrum is insensitive to further closeness of the spin labels in the open state at room temperature.

Based on our results, we propose the following mechanistic interpretation of the events associated with the conformational changes in the outer-vestibule of K^+ channels during C-type inactivation and how this leads to higher affinity Cd^{2+} binding (Figure 8). Cd^{2+} can bind to K^+ channels in the closed state (Figure 5), however, the formation of metal bridge is not possible due to geometric constraints of the outer-vestibule and the range of the dynamic fluctuations at the filter. Cd^{2+} therefore binds to individual cysteines (as in the crystal structure), which might represent the low-affinity binding state of Cd^{2+}. Upon opening the activation gate, the resulting conformational changes in the selectivity filter are driven by the network of interactions between the pore helix and the outer-vestibule (Cuello et al., 2010a). During the transition from open, conductive to open inactivated state, the residues in the outer-vestibule dynamically come close together (Figure 6) and Cd^{2+}, which was initially bound to individual subunits, rearranges to form a stable, high affinity metal bridges with the adjacent subunits (see Figures 3 and 7), thus stabilizing the inactivated state (Yellen et al., 1994). This model also supports the notion that a Cd^{2+} metal bridge can be formed only in the inactivated state of K^+ channels due to geometric constraints (see Figure 1E,F). In addition to the conformational transitions between the conductive and C-type inactivated forms of the selectivity filter, the presence of Cd^{2+} metal bridges between adjacent subunits just above the selectivity filter would enhance the rate of inactivation. Being a soft metal ion, Cd^{2+} coordination with –SH group of cysteine is not ionic, rather it is pseudo-covalent in nature (Elinder and Arhem, 2004). We therefore suggest that the two Cd^{2+} metal bridges formed at the outer-vestibule of KcsA might prevent side chain movement and the presence of partial positive charges in Cd-Sγ complexes might affect the electrostatic potential at the outer mouth of the channel that would interfere with K^+ ion permeation by electrostatic repulsion and thereby increasing the rate of inactivation.

Experimental Procedures

Cloning, Mutagenesis and Biochemistry

We used pQE32 vector encoding Y82C-KcsA and E71A/Y82C-KcsA genes for protein expression, as described (Cortes and Perozo, 1997). Tandem dimer (TD) Y82C-KcsA was constructed by cloning the Y82C-containing KcsA in B protomer of TD construct, and tandem tetramer (TT) Y82C-KcsA was made by cloning the Y82C-containing KcsA in C and D protomers of TT construct. The tandem constructs were expressed and purified as described previously (Liu et al., 2001; Liu, 2004). E71A mutation was carried out in Y82C background using QuickChange (Stratagene) site-directed mutagenesis. For EPR measurements, purified mutants were spinlabeled with methanethiosulfonate spinlabel (MTSSL, Toronto Research) and reconstituted in asolectin (Avanti Polar Lipids) vesicles as described previously (Liu et al., 2001). For distance measurements, we made full-labeled and under-labeled samples, and spin labeling was done at 1:10 (label/monomer) molar ratio to prepare under-label samples.

Wild-type *Shaker*-IR (ShΔ) tandem tetramer construct and the separate protomers (A B C D) were kindly provided by Dr. Yangyang Yan. We made TTCD-T449C construct by cloning T449C-containing ShΔ in C and D protomers using the appropriate restriction enzymes as described earlier (Yang et al., 1997). Tandem dimer (TD) Sh-IR was made from the TT-ShΔ

construct as follows: we digested TT ShΔ with ZraI (specific for the linker between A and B protomers) and EcoRV (specific for linker between C and D protomers) to remove B and C protomers and then used iProof DNA polymerase to extend the sticky end produced by EcoRV, followed by ligation to create a TD construct containing only A and D protomers of which only the D protomer has T449C mutation.

Liposome Patch-Clamp

Electrophysiological measurements of proteoliposomes were done using the patch-clamp as described earlier (Cordero-Morales et al., 2007). Macroscopic currents were measured at a 1:100 (wt/wt) ratio under symmetrical conditions in 5 mM MOPS, 200 mM KCl, pH 4.0 buffer after a pH jump using a RCS-160 fast-solution exchanger (Biologic). Pipette resistances were ∼2 MΩ. Cd^{2+} was used in the pipette solution at various concentrations.

Two-Electrode Voltage Clamp

We prepared cRNAs from ShΔ T449C and TD- and TT-T449C constructs using mMESSAGE mMACHINE T7 kit (Ambion) after linearization of plasmid cDNAs with Not I, and injected in *Xenopus laevis* oocytes (5 ng) cultured in ND96 medium supplemented with 50 ug ml^{-1} gentamycin and 1% (v/v) penicillin-streptomycin at 16 °C. We measured whole-cell currents 24 h after injection using a Geneclamp 500 amplifier (Axon instruments). The holding potential used was -90 mV and the currents in the absence and presence of 100 μM Cd^{2+} at +40 mV were measured for 8 s with a 30 s interval between pulses. Data were sampled at 5 kHz and recorded using Clampex software (Axon instruments). The bath solution was 10 mM HEPES containing 96 mM NaCl, 4 mM KCl, 1 mM $MgCl_2$, 0.3 mM $CaCl_2$, pH 7.6.

EPR Spectroscopy and Distance Calculations

Continuous-wave (CW) EPR spectra at room temperature were obtained for spin-labeled, reconstituted channels for closed (pH 7) and open (pH 4) channels as described earlier (Cordero-Morales et al., 2006b; 2007), using a Bruker EMX spectrometer equipped with a loop-gap resonator under the following conditions: 2 mW incident power, 100 kHz modulation frequency and 1 G modulation amplitude. pH changes were made by resuspending the KcsA-containing liposomes in Tris, KCl buffer for pH 7 and citrate phosphate buffer for pH 4. Distance measurements in closed and open states were made in proteoliposomes at 130 K in presence of liq. N_2 using <50 μW incident power to avoid the saturation of the signal. Full-label and under-label spectra are measured under identical conditions and distances were estimated using a dipolarly broadened CW spectra analysis program CWdipol (Sen et al., 2007).

X-ray Crystallography

We crystallized Y82C-KcsA in Cd^{2+}-bound and spin label bound forms in the presence of a Fab fragment using the conditions as described (Zhou et al., 2001). The concentration of Cd^{2+} used was 100 μM. Beam-like crystals of KcsA-Fab complex appeared within few days in a sitting-drop containing 23%-26% (v/v) PEG 400, 50 mM magnesium acetate and 50 mM sodium acetate (pH 4.8-5.4) at 20 °C. Crystals diffracted to a Bragg spacing of 2.4 Å and 2.5 Å for Cd^{2+}-bound and spinlabel-bound Y82C-KcsA, respectively. Data were collected at the GM/CA-24-ID beamline at the Advanced Photon Source and processed with HKL2000. The structures were solved by molecular replacement using the WT-KcsA-Fab complex structure (PDB: 1K4C) as a search model. All the structures were solved using Fab and KcsA without the selectivity filter as the initial model for molecular replacement. Refinement of the structures was carried out through multiple cycles of manual rebuilding

using O (Jones et al., 1991) and refinement using CNS (Brunger et al., 1998). Data collection and refinement statistics are given in Table 1.

Molecular Dynamics

The simulation system was represented by an atomic model of KcsA channel (PDB: 1K4D, low K^+ structure; Zhou et al., 2001) with Tyr82 in each of the four subunits mutated to a deprotonated cysteine *in silico*. The channel was embedded in dipalmitoylphosphatidylcholine (DPPC) lipids and surrounded by an aqueous solution of 150 mM KCl. The model contained the KcsA tetramer (404 amino acids), 112 DPPC molecules, 6,778 water molecules, $2K^+$ ions in the pore at positions S1 and S4, and a Cd^{2+} ion. To ensure electrical neutrality and to mimic a 150 mM KCl concentration, 6 K^+ and 18 Cl^- ions were added to the bulk solution. The system was set up using CHARMM program (Brooks et al., 2009) as described earlier (Berneche and Roux, 2000). Constant pressure molecular dynamics simulation was done using the NAMD program (Phillips et al., 2005).

The brute force simulations in Figure 4A were run for 350 ps. The initial conformation was prepared by adding a harmonic restraining potential that enforced the distance between the cadmium and the sulfur atoms of the diagonal Cys82 residues to be 2.5 Å. For adjacent coordination, a similar procedure was used to prepare the initial conformation except the harmonic restraints were applied between cadmium and adjacent Cys82 residues. These restraints were turned off during brute force simulations. The free energy difference between the adjacent and diagonally opposing states (Figure 4B) was calculated by measuring the mean force at several points along an intervening conformational change pathway. Starting from a conformation where distances between the cadmium ion and two adjacent Y82C sulfur atoms were 2.5 Å and the distance between the cadmium and one of the diagonal Y82C sulfur atoms was 15.5 Å, the ion was linearly pulled to a final conformation where it was 2.5 Å away from two diagonally opposing Y82C sulfur atoms and 9.5 Å away from the adjacent Y82C sulfur atom to which it was originally coordinated. The pathway proceeded in 0.5 Å increments using 15 images with a sampling time of 50 ps per image. The total free energy difference was then determined by integrating the mean force along the path as described previously (Maragliano et al., 2006; Pan et al., 2008). Although the pathway itself may not be physically relevant, the relative free energy between the two states is path-independent.

Supplementary Material

Refer to Web version on PubMed Central for supplementary material.

Acknowledgments

We thank Sudha Chakrapani and Raymond Bourdeau for critical reading and comments on the manuscript; Y. Yan and F.J. Sigworth (Yale University) for wild type *Shaker*-IR (ShΔ) tandem tetramer construct and the separate protomers (A B C D); R. MacKinnon (Rockefeller University) for providing the Fab-expressing hybridoma cells; D.M. Cortes for Fab preparations; S. Goldstein (University of Chicago) for providing access to the two-electrode voltage clamp system. We are thankful to the staff at the NE-CAT 24ID and GM-CA 23ID beamlines at the Advanced Photon Source, Argonne National Laboratory. This work was supported in part by NIH grants R01-GM57846, and U54 GM74946.

References

Ader C, et al. A structural link between inactivation and block of a K^+ channel. Nat Struct Mol Biol. 2008; 15:605–612. [PubMed: 18488040]

Alam A, Jiang Y. High-resolution structure of the open NaK channel. Nature Struct Mol Biol. 2009; 16:30–34. [PubMed: 19098917]

Andalib P, Consiglio JF, Trapani JG, Korn SJ. The external TEA binding site and C-type inactivation in voltage-gated potassium channels. Biophys J. 2004; 87:3148–3161. [PubMed: 15326027]

Baukrowitz T, Yellen G. Modulation of K+ current by frequency and external [K^+]: a tale of two inactivation mechanisms. Neuron. 1995; 15:951–960. [PubMed: 7576643]

Bean BP. The action potential in mammalian central neurons. Nat Rev Neurosci. 2007; 8:451–465. [PubMed: 17514198]

Berneche S, Roux B. Molecular dynamics of the KcsA K^+ channel in a bilayer membrane. Biophys J. 2000; 78:2900–2917. [PubMed: 10827971]

Berneche S, Roux B. A gate in the selectivity filter of potassium channels. Structure. 2005; 13:591–600. [PubMed: 15837197]

Blunk R, Cordero-Morales JF, Cuello LJ, Perozo E, Bezanilla F. Detection of the opening of the bundle crossing in KcsA with fluorescence lifetime spectroscopy reveals the existence of two gates for ion conduction. J Gen Physiol. 2006; 128:569–581. [PubMed: 17043150]

Brooks BR, et al. CHARMM: the biomolecular simulation program. J Comput Chem. 2009; 30:1545–1614. [PubMed: 19444816]

Brunger T, et al. Crystallography and NMR system: a new software suite for macromolecular structure determination. Acta Crystallogr D Biol Crystallogr. 1998; 54:905–921. [PubMed: 9757107]

Cha A, Bezanilla F. Characterizing voltage-dependent conformational changes in the *Shaker* K^+ channel with fluorescence. Neuron. 1997; 19:1127–1140. [PubMed: 9390525]

Chakrapani S, Cordero-Morales JF, Jogini V, Pan A, Cortes DM, Roux B, Perozo E. On the structural basis of modal gating behavior in K+ channels. Nat Struct Mol Biol. 2011; 18:67–74. [PubMed: 21186363]

Choi KL, Aldrich RW, Yellen G. Tetraethylammonium blockade distinguishes two inactivation mechanisms in voltage-activated K+ channels. Proc Natl Acad Sci USA. 1991; 88:5092–5095. [PubMed: 2052588]

Claydon TW, Makary SY, Dibb KM, Boyett MR. The selectivity filter may act as the agonist-activated gate in the G protein activated-Kir3.1/Kir3.4 K^+ channel. J Biol Chem. 2003; 278:50654–50663. [PubMed: 14525972]

Cordero-Morales JF, Cuello LG, Perozo E. Voltage-dependent gating at the potassium channel selectivity filter. Nat Struct Mol Biol. 2006a; 13:319–322. [PubMed: 16532008]

Cordero-Morales JF, Cuello LG, Zhao Y, Jogini V, Cortes DM, Roux B, Perozo E. Molecular determinants of gating at the potassium channel selectivity filter. Nat Struct Mol Biol. 2006b; 13:311–318. [PubMed: 16532009]

Cordero-Morales JF, Jogini V, Lewis A, Vasquez V, Cortes DM, Roux B, Perozo E. Molecular driving forces driving potassium channel slow inactivation. Nat Struct Mol Biol. 2007; 14:1062–1069. [PubMed: 17922012]

Cordero-Morales JF, Jogini V, Chakrapani S, Perozo E. A multipoint hydrogen-bond network underlying KcsA C-type inactivation. Biophys J. 2011; 100:2387–2393. [PubMed: 21575572]

Cortes DM, Perozo E. Structural dynamics of the *Streptomyces lividans* K^+ channel (SKC1): oligomeric stoichiometry and stability. Biochemistry. 1997; 36:10343–10352. [PubMed: 9254634]

Cuello LG, Jogini V, Cortes DM, Perozo E. Structural mechanism of C-type inactivation in K+ channels. Nature. 2010a; 466:203–208. [PubMed: 20613835]

Cuello LG, Jogini V, Cortes DM, Pan AC, Gagnon DH, Dalmas O, Cordero-Morales JF, Chakrapani S, Roux B, Perozo E. Structural basis for the coupling between activation and inactivation gates in K(+) channels. Nature. 2010b; 466:272–275. [PubMed: 20613845]

Demo SD, Yellen G. Ion effects on gating of the Ca^{2+}-activated K^+ channel correlate with occupancy of the pore. Biophys J. 1992; 61:639–648. [PubMed: 1504240]

Elinder F, Arhem P. Metal ion effects on ion channel gating. Q Rev Biopys. 2004; 36:373–427.

Gandhi CS, Loots E, Isacoff EY. Reconstructing voltage sensor-pore interaction from a fluorescence scan of a voltage-gated K^+ channel. Neuron. 2000; 27:585–595. [PubMed: 11055440]

Gao L, Mi X, Paajanen V, Wang K, Fan Z. Activation-coupled inactivation in the bacterial potassium channel KcsA. Proc Natl Acad Sci USA. 2005; 102:17630–17635. [PubMed: 16301524]

Heginbotham L, MacKinnon R. The aromatic binding site for tetraethylammonium ion in potassium channels. Neuron. 1992; 8:483–491. [PubMed: 1550673]

Hoshi T, Zagotta WN, Aldrich RW. Biophysical and molecular mechanisms of *Shaker* potassium channel inactivation. Science. 1990; 250:533–538. [PubMed: 2122519]

Hoshi T, Zagotta WN, Aldrich RW. Two types of inactivation in *Shaker* K+ channels: effects of alterations in the carboxy-terminal region. Neuron. 1991; 7:547–556. [PubMed: 1931050]

Hurst RS, Kavanaugh MP, Yakel J, Adelman JP, North RA. Cooperative interactions among subunits of voltage-dependent potassium channel. Evidence from expression of concatenated cDNAs. J Biol Chem. 1992; 267:23742–23745. [PubMed: 1385425]

Jiang Y, Lee A, Chen J, Cadene M, Chait BT, MacKinnon R. The open pore conformation of potassium channels. Nature. 2002; 417:523–526. [PubMed: 12037560]

Jones TA, Zou JY, Cowan SW, Kjeldgaard M. Improved methods for building protein models in electron density maps and the location of errors in these models. Acta Crystallogr A. 1991; 47:110–119. [PubMed: 2025413]

Kurata HT, Fedida D. A structural interpretation of voltage-gated potassium channel inactivation. Prog Biophys Mol Biol. 2006; 92:185–208. [PubMed: 16316679]

Liu Y, Jurman ME, Yellen G. Dynamic rearrangement of the outer mouth of a K^+ channel during gating. Neuron. 1996; 16:859–867. [PubMed: 8608004]

Liu, YS. PhD Dissertation. University of Virginia; 2004. Gating Mechanism of Potassium Channels Studied by Electron Paramagnetic Resonance Spectroscopy.

Liu YS, Sompornpisut P, Perozo E. Structure of the KcsA channel intracellular gate in the open state. Nat Struct Biol. 2001; 8:883–887. [PubMed: 11573095]

Lockless SW, Zhou M, MacKinnon R. Structural and thermodynamic properties of selective ion binding in a K^+ channel. PLoS Biol. 2007; 5:e121. [PubMed: 17472437]

Long SB, Campbell EB, MacKinnon R. Crystal structure of a mammalian voltage-dependent Shaker family K^+ channel. Science. 2005; 309:897–903. [PubMed: 16002581]

Loots E, Isacoff EY. Protein rearrangements underlying slow inactivation of the *Shaker* K^+ channel. J Gen Physiol. 1998; 112:377–389. [PubMed: 9758858]

Loots E, Isacoff EY. Molecular coupling of S4 to a K^+ channel's slow inactivation gate. J Gen Physiol. 2000; 116:623–635. [PubMed: 11055991]

Lopez-Barneo J, Hoshi T, Heinemann SH, Aldrich RW. Effects of external cations and mutations in the pore region on C-type inactivation of Shaker potassium channels. Receptors Channels. 1993; 1:61–71. [PubMed: 8081712]

Maragliano L, Fischer A, Vanden-Eijnden E, Cicotti G. String method in collective variables: minimum free energy paths and isocommittor surfaces. J Chem Phys. 2006; 125:24106. [PubMed: 16848576]

Narula SS, Brouwer M, Hua Y, Armitage IM. Three-dimensional solution structure of *Callinectes sapidus* metallothionein-1 determined by homonuclear magnetic resonance spectroscopy. Biochemistry. 1995; 34:620–631. [PubMed: 7819257]

Naylor CE, Eaton JT, Howells A, Justin N, Moss DS, Titball RW, Basak AK. Structure of the key toxin in gas gangrene. Nat Struct Biol. 1998; 5:738–746. [PubMed: 9699639]

Ogielska EM, Zagotta WN, Hoshi T, Heinemann SH, Haab J, Aldrich RW. Cooperative subunit interactions in C-type inactivation of K channels. Biophys J. 1995; 69:2449–2457. [PubMed: 8599651]

Pan AC, Sezer D, Roux B. Finding transition pathways using the string method with swarms of trajectories. J Phys Chem B. 2008; 112:3432–3440. [PubMed: 18290641]

Perozo E, Cortes DM, Cuello LG. Three-dimensional architecture and gating mechanism of a K^+ channel studied by EPR spectroscopy. Nat Struct Biol. 1998; 5:459–469. [PubMed: 9628484]

Perozo E, Cortes DM, Cuello LG. Structural rearrangements underlying K^+-channel activation gating. Science. 1999; 285:73–78. [PubMed: 10390363]

Phillips JC, Braun R, Wang W, Gumbart J, Tajkhorshid E, Villa E, Chipot C, Skeel RD, Kale L, Schulten K. Scalable molecular dynamics with NAMD. J Comput Chem. 2005; 26:1781–1802. [PubMed: 16222654]

Schlief T, Schonherr R, Heinemann SH. Modification of C-type inactivating Shaker potassium channels by chloramine-T. Pflugers Arch. 1996; 431:483–493. [PubMed: 8596690]

Sen KI, Logan TM, Fajer PG. Protein dynamics and monomer-monomer interactions in AntR activation by electron paramagnetic resonance and double electron-electron resonance. Biochemistry. 2007; 46:11639–11649. [PubMed: 17880108]

Shealy RT, Murphy AD, Ramarathnam R, Jakobsson E, Subramaniam S. Sequence-function analysis of the K^+-selective family of ion channels using a comprehensive alignment and the KcsA channel structure. Biophys J. 2003; 84:2929–2942. [PubMed: 12719225]

Smith PL, Baukrowitz T, Yellen G. The inward rectification mechanism of the HERG cardiac potassium channel. Nature. 1996; 379:833–836. [PubMed: 8587608]

Sobolevsky AI, Yelshansky MV, Wollmuth LP. The outer pore of the glutamate receptor channel has 2-fold rotational symmetry. Neuron. 2004; 41:367–378. [PubMed: 14766176]

Spector PS, Curran ME, Zou A, Keating MT, Sanguinetti MC. Fast inactivation causes rectification of the IKr channel. J Gen Physiol. 1996; 107:611–619. [PubMed: 8740374]

Swenson RP, Armstrong CM. K+ channels close more slowly in the presence of external K^+ and Rb^+ Nature. 1981; 291:427–429. [PubMed: 6264306]

Szendroedi J, Sandtner W, Zarrabi T, Zebedin E, Hilber K, Dudley SC Jr, Fozzard HA, Todt H. Speeding the recovery from ultraslow inactivation of voltage-gated Na^+ channels by metal ion binding to the selectivity filter: A foot-*on*-the-door? Biophys J. 2007; 93:4209–4224. [PubMed: 17720727]

Yang Y, Yan Y, Sigworth FJ. How does the W434F mutation block current in *Shaker* potassium channels? J Gen Physiol. 1997; 109:779–789. [PubMed: 9222903]

Yellen G. The moving parts of voltage-gated ion channels. Q Rev Biophys. 1998; 31:239–295. [PubMed: 10384687]

Yellen G, Sodickson D, Chen TY, Jurman ME. An engineered cysteine in the external mouth allows inactivation to be modulated by metal binding. Biophys J. 1994; 66:1068–1075. [PubMed: 8038379]

Zhou Y, Morais-Cabral JH, Kaufman A, MacKinnon R. Chemistry of ion coordination and hydration revealed by a K+ channel-Fab complex at 2.0 Å resolution. Nature. 2001; 414:43–48. [PubMed: 11689936]

- Cd^{2+} metal bridges in the outer-vestibule enhance the rate of inactivation in K^+ channels
- Cd^{2+} metal bridges are formed only between adjacent subunits
- Metal bridge formation is a two-step process
- Subunits come dynamically closer as the channels inactivate

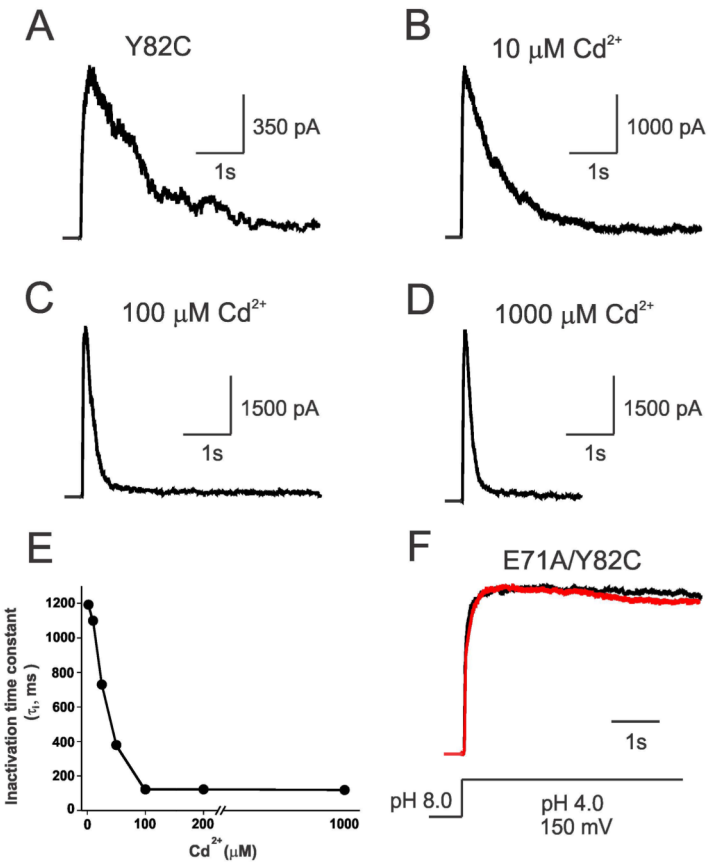

Figure 1. Cd^{2+} Increases the Rate of Inactivation in Y82C-KcsA

Normalized macroscopic currents of Y82C mutant of KcsA, reconstituted in asolectin liposomes, at a depolarizing potential (+150 mV) for concentrations of Cd^{2+} ranging from 0 to 1 mM (A-D); in the background of non-inactivating mutant E71A in the presence (red) and absence (black) of 100 μM Cd^{2+} (F). Macroscopic responses of Y82C-KcsA under various conditions were elicited by pH jumps from 8.0 to 4.0 using a rapid solution exchanger in the presence of 200 mM KCl and with a membrane potential held at +150 mV. Inactivation time constant (τ_i) as a function of various Cd^{2+} concentrations is shown in (E), n > 5.

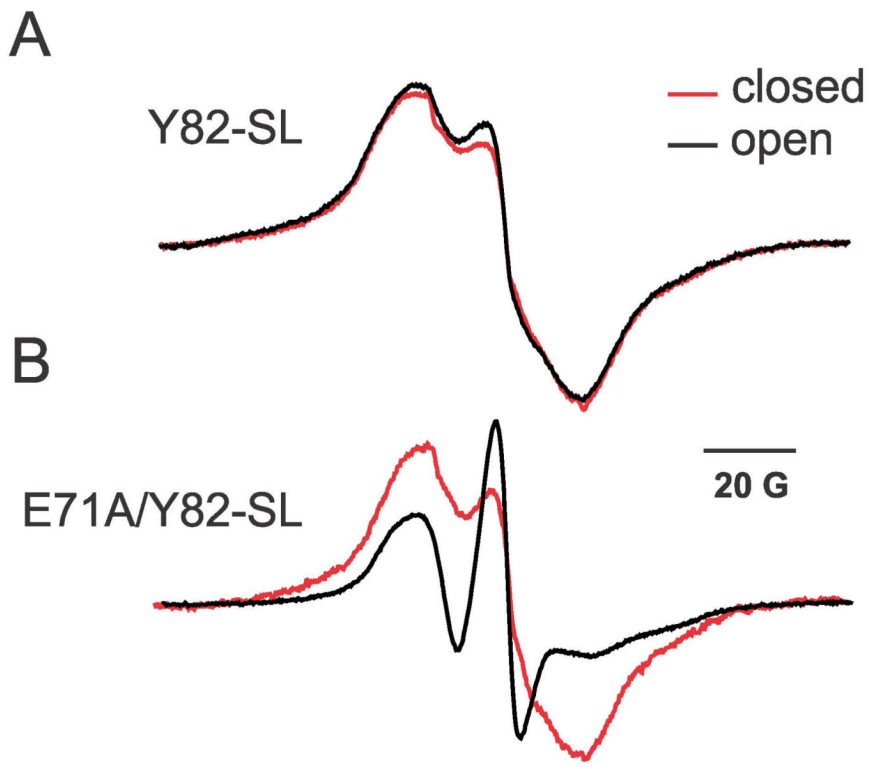

Figure 2. Mobility Differences of Spin-labeled Y82C in Reconstituted WT and E71A Channels

Effect of opening the lower gate on the mobility of spin-labeled outer-vestibule residue Y82C in reconstituted wild type (top) and non-inactivating mutant E71A (bottom) backgrounds for the closed (pH 7, red) and open (pH4, black) states of KcsA, as determined by CW-EPR.

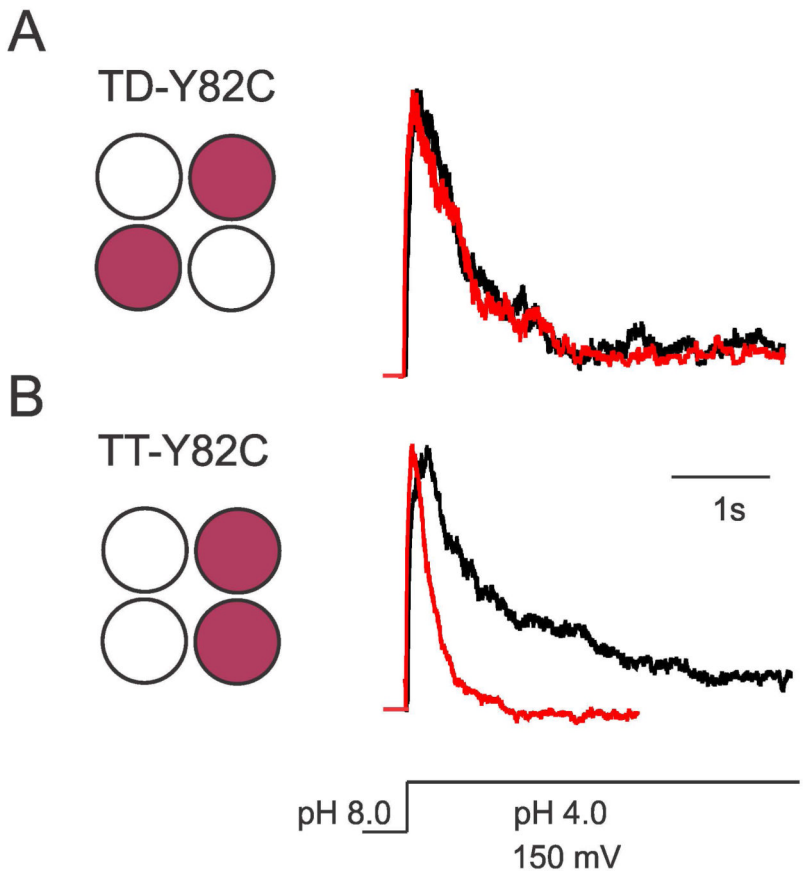

Figure 3. Cd^{2+}Metal Bridge is Formed between Adjacent Subunits

Normalized currents of (A) TD-Y82C (diagonal cysteines) and (B) TT-Y82C-KcsA (adjacent cysteines), reconstituted in asolectin liposomes, in the absence (black) and presence of 100 μM Cd^{2+} (red). Macroscopic responses of tandem constructs were elicited by pH jumps from 8.0 to 4.0 using a rapid solution exchanger in the presence of 200 mM KCl and with a membrane potential held at +150 mV, n > 5. A schematic representation of the position of cysteines in the TD (tandem dimer) and TT (tandem tetramer) constructs of Y82C-KcsA is shown.

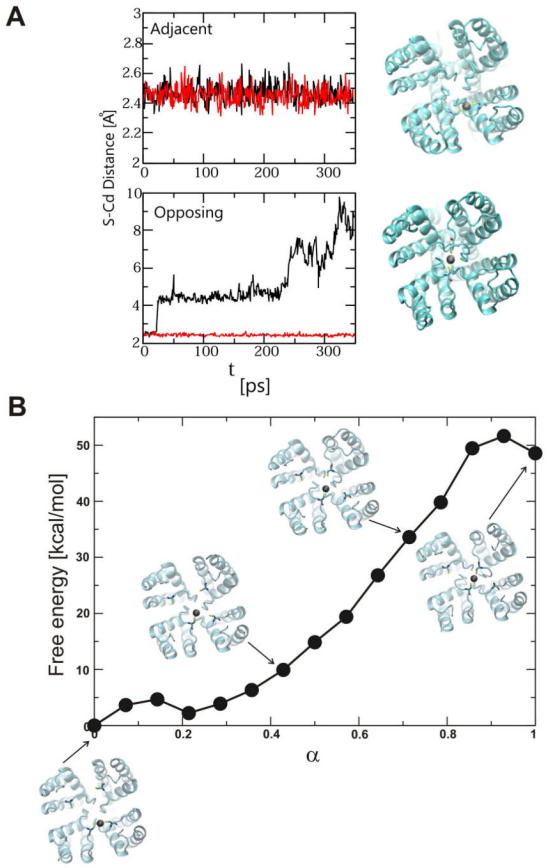

Figure 4. Stability of Cd^{2+}Coordinated States

(A) Change in S-Cd^{2+} distance during brute force molecular dynamics simulations (350 ps) in Y82C-KcsA for Cd^{2+} coordinated initially between adjacent (top) and diagonal (bottom) configurations. Snapshots of initial and final configurations are shown in top view. (B) Change in free energy for linearly pulling Cd^{2+} from a coordination state between adjacent subunits to a coordination state between diagonal subunits. Snapshots of configurations along the path are shown. Cadmium is represented by a grey sphere, and side chains of Y82C for the relevant two subunits are shown in sticks. See Experimental Procedures and text for details, and Supplementary Movies online.

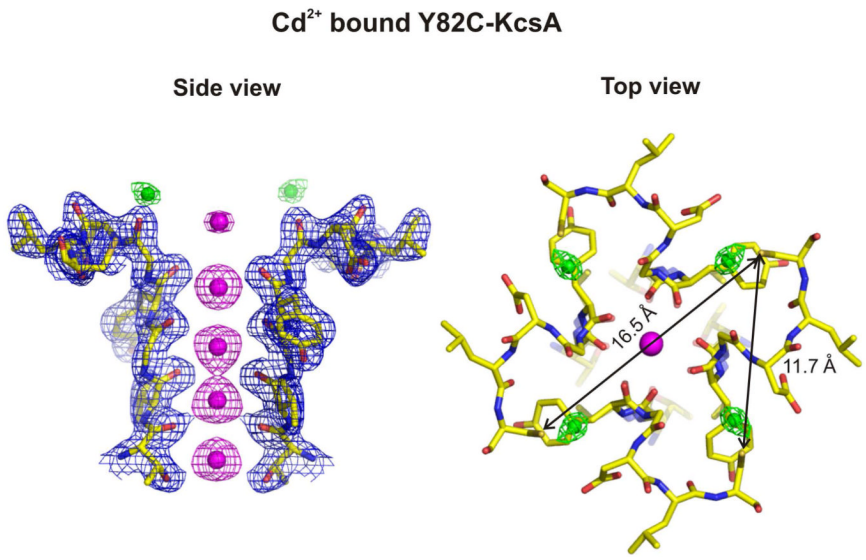

Figure 5. Crystal structure of the Cd^{2+}-bound Y82C-KcsA at 2.4 Å resolution

Shown are the $2F_o$-F_c electron density map of the side view for diagonally symmetric subunits [left; sigma for protein (blue mesh) = 2.0, sigma for potassium (magenta mesh) = 2.5, sigma for cadmium (green mesh) = 3.2] and top view (right) of the tetramer structure depicting the individually bound Cd^{2+} (green spheres) to Y82C cysteines. The polypeptide chain is shown as sticks. The S_γ-S_γ distances between cysteines corresponding to diagonal and adjacent subunits are shown (black arrows). See Experimental Procedures and text for details.

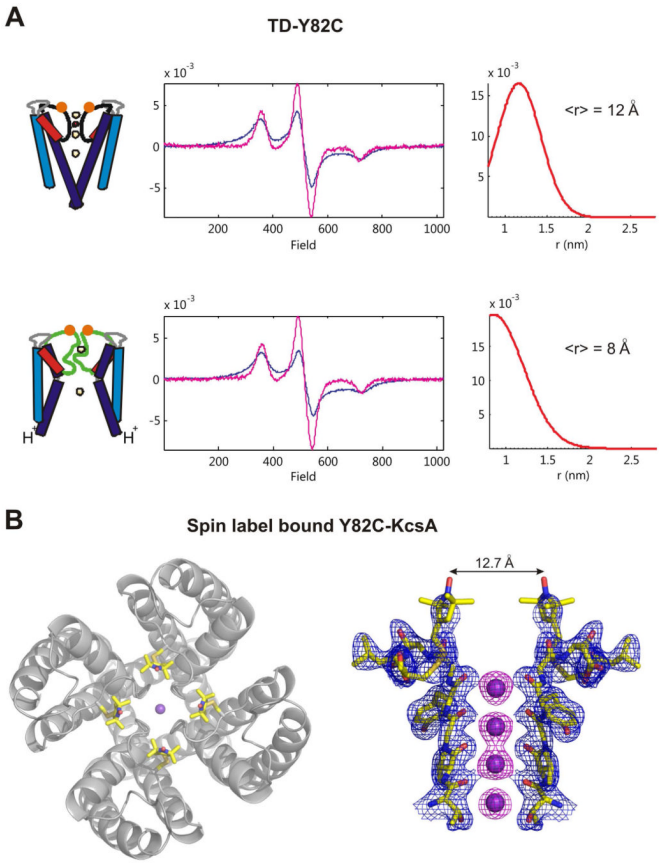

Figure 6. Subunits come closer dynamically during inactivation gating

(A) CW-EPR distance determination between spin labels bound to diagonally placed Y82C in TD KcsA in the closed (pH 7, top) and open (pH 4, bottom) forms of KcsA. Distance measurements were made in proteoliposomes at 130 K in the presence of liq. N_2 using <50 μW incident power to avoid saturation of the signal. The full and under label EPR spectra are shown in the left, and the probability of distance distributions with the mean distance is shown on right. A cartoon depicting the closed and opened tandem dimer channels as well as the position of spinlabeled Y82C in the outer-vestibule is shown. (B) The crystal structure of spinlabel-bound Y82C-KcsA tetramer at 2.5 Å is shown (left, top view) along with the $2F_o$-F_c electron density map of the side view for diagonally symmetric subunits [right; sigma for protein (blue mesh) = 2.0, sigma for potassium (magenta mesh) = 2.5] depicting the spinlabel bound to Y82C cysteines. The polypeptide chain is shown as sticks. The distance between the N-O groups of the spinlabel (12.7 Å) from two diagonally symmetric subunits is shown (black arrow). See Experimental Procedures and text for details.

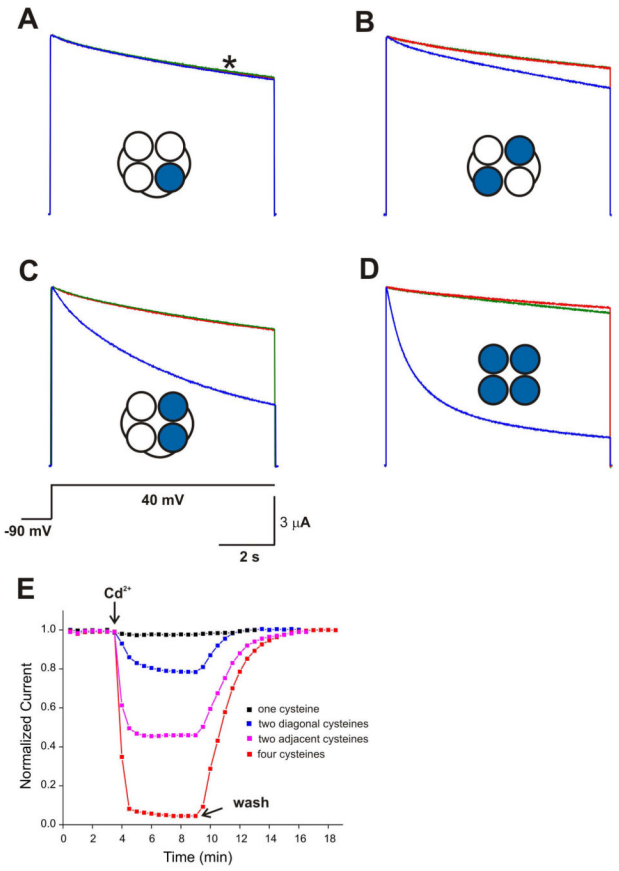

Figure 7. Cd^{2+} metal bridge formation between adjacent subunits is highly favorable in *Shaker* K^+ channels

Two-electrode voltage clamp measurements for various ShΔ T449C constructs expressed in oocytes corresponding to channels in which (A) cysteine is present in only one subunit (TTCT); (B) cysteines in diagonal subunits (TC); (C) cyseines in adjacent subunits (TTCC) and (D) cysteines in all subunits (T449C monomer). The traces represent the current recordings during 8 s depolarizations to +40 mV in the absence (red) and presence of 100 μM Cd^{2+} (blue) and subsequent wash (green). Inset shows the cartoon representation of channels highlighting the subunit containing T449C mutations (blue). The holding potential was -90 mV and the time interval between pulses is 30 s. n > 5. A star represents the point where the amplitude of current is measured for each pulse in all cases. The effect of Cd^{2+} on inactivation kinetics in ShΔ T449C constructs is shown in (E) for TTCT (black squares); TC (blue squares); TTCC (majenta squares) and T449C monomer (red squares). See Experimental Procedures for details.

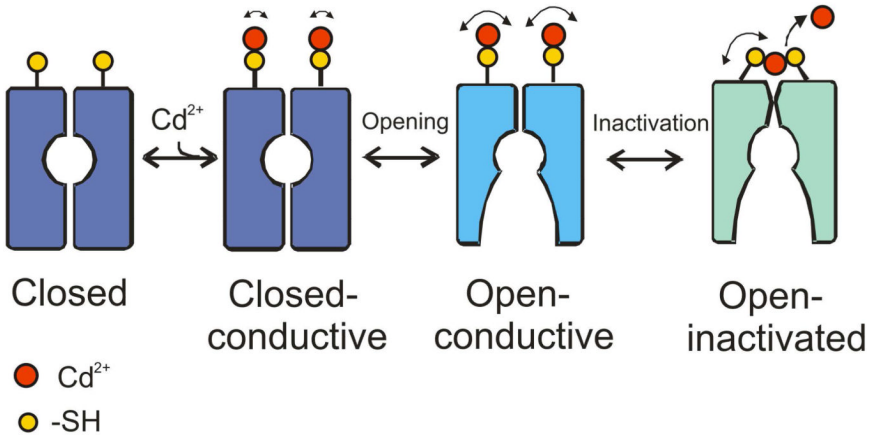

Figure 8. Mechanism of stabilization of inactivated state by Cd^{2+}

Addition of Cd^{2+} binds to individual cysteines at the outer-vestibule in the closed state. When the channel is opened, Cd^{2+} rearranges to form favorable metal bridges with cysteines of adjacent subunits due to structural rearrangements of the outer-vestibule. This possibly stabilizes the C-type inactivated state and results in decrease in the K^+ current amplitude and increase in the rate of inactivation in K^+ channels. Our model suggests that formation of the Cd^{2+} metal bridge is absolutely essential to affect the rate of C-type inactivation, and the formation of metal bridge is favored only in the inactivated state. See Discussion for details.

Table 1

Crystallographic Data Collection and Refinement Statistics

	Y82C-Cd^{2+}	**Y82C-SL**
Data collection		
Space group	I4	I4
Cell dimensions		
a=*b*, *c* (Å)	155.9,76.1	155.7, 76.1
$\alpha=\beta=\gamma$ (°)	90	90
Resolution (Å)	40-2.4	40-2.5
R_{sym} or R_{merge} (%)	8.1(28.5)	8.2(47.4)
$I/\sigma I$	13.3(1.7)	13.8(3.2)
Completeness (%)	93.5	92.9
Redundancy	2.9(1.9)	5.2(4.3)
Refinement		
Resolution (Å)	40-2.4	40-2.5
No. reflections	33542	29442
R_{work}/R_{free} (%)	22.7/26.5	24.6/28.5
No. atoms		
Protein	4065	4062
Ligand/ion	7	5
Water	3	4
B-factors		
Protein	44.7	46.4
Ligand/ion	41.4	29.5
Water	37.8	42.21
R.m.s deviations		
Bond lengths (Å)	0.007	0.007
Bond angles (°)	1.34	1.41